

# Efficient Bayesian inversion for shape reconstruction of lithography masks

Nando Farchmin<sup>a,b</sup>, Martin Hammerschmidt<sup>c,d</sup>, Philipp-Immanuel Schneider<sup>c,d</sup>, Matthias Wurm<sup>a</sup>, Bernd Bodermann<sup>a</sup>, Markus Bär<sup>a</sup>, and Sebastian Heidenreich<sup>a</sup>

<sup>a</sup>Physikalisch-Technische Bundesanstalt, Braunschweig and Berlin

<sup>b</sup>Technische Universität Berlin, Institute of Mathematics

<sup>c</sup>JCMwave GmbH

<sup>d</sup>Zuse Institute Berlin

## ABSTRACT

**Background:** Scatterometry is a fast, indirect and non-destructive optical method for quality control in the production of lithography masks. To solve the inverse problem in compliance with the upcoming need for improved accuracy, a computationally expensive forward model has to be defined which maps geometry parameters to diffracted light intensities.

**Aim:** To quantify the uncertainties in the reconstruction of the geometry parameters, a fast to evaluate surrogate for the forward model has to be introduced.

**Approach:** We use a non-intrusive polynomial chaos based approximation of the forward model which increases speed and thus enables the exploration of the posterior through direct Bayesian inference. Additionally, this surrogate allows for a global sensitivity analysis at no additional computational overhead.

**Results:** This approach yields information about the complete distribution of the geometry parameters of a silicon line grating, which in return allows to quantify the reconstruction uncertainties in the form of means, variances and higher order moments of the parameters.

**Conclusion:** The use of a polynomial chaos surrogate allows to quantify both parameter influences and reconstruction uncertainties. This approach is easy to use since no adaptation of the expensive forward model is required.

**Keywords:** uncertainty quantification, polynomial chaos, inverse problem, parameter reconstruction, scatterometry

## ACKNOWLEDGEMENTS

This project has received funding from the German Central Innovation Program (ZIM) No. ZF4014017RR7.

## 1. INTRODUCTION

Scatterometry is an optical scattering technique frequently used for the characterization of periodic nanostructures on surfaces in semiconductor industry (determination of critical dimensions).<sup>1-4</sup> In contrast to other techniques like electron microscopy, optical microscopy or atomic force microscopy, scatterometry is a non-destructive and indirect method. In the last decades both feature sizes and the required measurement uncertainty decreased continuously, hence advanced scatterometry techniques are required. Recently, deep ultraviolet (DUV) scatterometry,<sup>5-7</sup> extreme ultraviolet (EUV) scatterometry,<sup>1,8</sup> imaging scatterometry<sup>9</sup> and combinations with white light interferometry<sup>10</sup> are developed. In these approaches, geometrical parameters and associated uncertainties can be determined from diffraction patterns by solving a statistical inverse problem.<sup>11</sup> For an overview on the metrology of surfaces in semiconductor industry see<sup>12</sup> and references therein.

We emphasize that scatterometry is an integral measurement method, which means that information of variances within the probe are lost due to an averaging over the spot size of the beam. These parameter variations

---

E-mail: nando.farchmin@ptb.de

typically lead to a broadening of the diffracted beam. This stochastic effect was not taken into account by the model of the line structure used in this work. Instead the diffraction efficiencies were calculated from the integral over the whole beam.

The inverse problem of scatterometry is in general ill-posed and regularization techniques have to be applied. The geometry is typically parametrized and sought-after parameters are obtained by weighted least squares minimization,<sup>13</sup> with weights derived directly from uncertainties in the measurements. However, the quality of these weights depends highly on the measurements used and itself influences the reconstruction results of the geometry parameters.<sup>14</sup> An alternative approach is to apply a maximum likelihood estimate, which introduces a likelihood function based on an error model and optimizes weighting terms as hyper parameters instead of using predefined values. Based on the same principle but additionally including some prior knowledge is the maximum posterior approach, which is a state of the art method in parameter reconstructions.<sup>15</sup> In the above frameworks, uncertainties are typically obtained from the Fischer information or covariance matrix, which relies on an assumed shape of the posterior. However, the shape of the posterior is generally unknown, hence this can lead to significant errors in the estimation of uncertainties if the actual posterior shape differs from the assumed one.

The Bayesian approach allows to integrate prior knowledge<sup>16</sup> and approximates the probability density function of the geometry parameters independent of any shape assumptions. Uncertainties obtained by employing Bayesian inference are thus much more robust. On the other hand it requires a large number of evaluations of the forward model which is not feasible for expensive computations as in the case of scatterometry. To obtain a surrogate model that mitigates the computation time, we employ a polynomial chaos expansion, that is an expansion into an orthonormal polynomial basis in the parameter space to approximate the forward model with a global polynomial.<sup>17,18</sup> We additionally show how this surrogate allows for a Bayesian approach to the inverse problem.

In a recent publication, it has been demonstrated that a surrogate of a forward model for scatterometry based on a polynomial chaos expansion enables Bayesian inversion and the use of Markov Chain Monte Carlo (MCMC) sampling. In this approach, cubature rules on sparse grids of Smolyak type are used to determine the expansion coefficients and to construct the surrogate model.<sup>19,20</sup> However, cubature rules and sparse grids are adapted to the stochastic distributions chosen and less accurate for correlated stochastic input parameters. In the present work we used optimal linear regression to obtain the coefficients of the polynomial chaos expansion. This novel approach uses optimal sampling points, is much more flexible and well suited for extensions to adaptive systems.

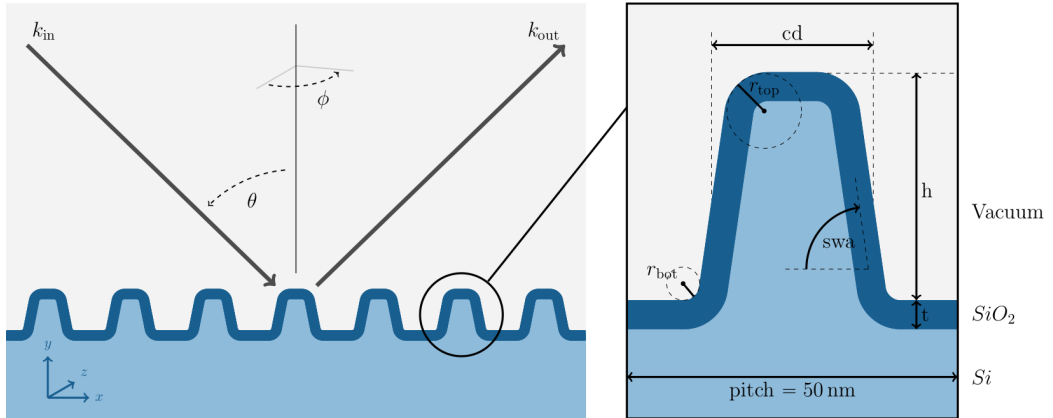


Figure 1. Cross section of the photomask with description of the stochastic parameters. The dimensional parameter vector is given by  $\xi = (h, cd, swa, t, r_{top}, r_{bot})$ . The pitch of the computational domain, i.e. the period is fixed to 50 nm.

In this paper, we determine the geometry parameters of a photomask that consists of multilayered, periodic, straight absorber lines of two optically different materials. The period of the line structure (pitch) is 50 nm and the geometry parameters of interest are the height of the line  $h$ , the width at the middle of the line (critical

dimension) CD, the sidewall angle SWA, the silicon oxide layer thickness  $t$  and the radii of the rounding at the top and bottom corners of the line  $r_{\text{top}}$  and  $r_{\text{bot}}$ , respectively. A cross section of the geometry for one period of the structure is depicted in Fig. 1. The photomask was illuminated by a light beam of wavelength  $\lambda = 266$  nm (DUV) for different angles of incidence  $\theta = 3^\circ, 5^\circ, \dots, 87^\circ$  for perpendicular ( $\phi = 0^\circ$ ) and parallel ( $\phi = 90^\circ$ ) orientation of the beam with respect to the grating structure as well as S and P polarization. The refractive indices used are  $n_{\text{si}} = 1.967 + 4.443i$  for silicon,  $n_{\text{ox}} = 1.7212 + 0.113i$  for the top oxide layer and  $n_{\text{air}} = 1.0$  for air. All the materials are assumed to be isotropic and non-magnetic ( $\mu_r = 1.0$ ).

In the next sections, we will proceed as follows. First, we introduce the forward model of the problem. Second, we describe a non-intrusive method to build a polynomial chaos based surrogate by utilizing an optimal sampling strategy. In Section 4 and 5 we apply Bayesian inversion to our surrogate. Finally, we estimate the posterior distribution from measurement data and compare the results.

## 2. FORWARD MODEL

In principle, the propagation of electromagnetic waves is described by Maxwell's equations, but for our simple grating geometry and in the time-harmonic case, Maxwell's equations reduce to a single second order partial differential equation,<sup>15,21</sup>

$$\nabla \times \mu(r)^{-1} \nabla \times E(r) - \omega^2 \varepsilon(r) E(r) = 0. \quad (1)$$

Here,  $\varepsilon$  and  $\mu$  are the permittivity and permeability,  $r$  is the spatial coordinate and  $\omega$  is the frequency of the incoming beam. We employ the finite element method (FEM)<sup>21</sup> implemented in the JCMSuite software package to discretize and solve the corresponding scattering problem formulation on a bounded computational unit cell in weak formulation as described in.<sup>22</sup> This formulation yields a splitting of the complete  $\mathbb{R}^n$  into an interior domain hosting the total field (incident and scattered) and an exterior domain where only the purely outward radiating scattered field is present. Appropriate boundary conditions are applied at the boundary of the computational domain as depicted in Fig. 1. As the geometry is periodic in lateral direction Bloch-periodic boundary conditions are applied. In vertical direction the geometry is assumed to be unbounded and thus requires the satisfaction of a transparent boundary condition at the interface. We use an adaptive perfectly matched layer (PML) method<sup>23,24</sup> to realize the transparent boundary condition and to satisfy the radiation condition for the scattered field. The employed vectorial FE method uses high-order polynomial ansatz functions defined on the spatial discretization of the computational domain. The triangulation allows to geometrically resolve the material interfaces and the tangential continuity of the electromagnetic fields across these interfaces is automatically enforced by the method.

The forward model is given by a map of geometry parameters onto S and P polarization of zeroth order intensities of the scattered light. The parameters  $\xi$  used for modelling the grating geometry are depicted in Fig. 1. The forward model is represented by the function  $f^*: \Omega \rightarrow \mathbb{R}^d$  such that the parameters  $\xi \in \Omega \subset \mathbb{R}^M$  are mapped to diffracted efficiencies for a set of azimuthal angles, incidence angles and polarizations. Each of the  $d$  components of  $f(\xi)$  represents a different combination of azimuth, incidence angle and polarization. All other experimental conditions such as e.g. the wavelength are fixed for this forward model. In our approach, the experimental data  $y \in \mathbb{R}^d$  are modelled with the error  $y_j = f_j(\xi) + \varepsilon_j$ ,  $j = 1, \dots, d$  where  $\varepsilon_j \sim \mathcal{N}(0, \sigma_j)$  describes a normal distributed noise with zero mean, standard deviation and error parameter  $b$ ,

$$\sigma_j(b) = b y_j, \quad \text{for } b > 0. \quad (2)$$

Choosing  $\sigma_j$  to depend on a stochastic parameter itself instead of setting it to specific values allows for an estimation of the measurement error based on the measurement data in the parameter reconstruction and thus incorporates less prior knowledge. The inverse problem is defined as the determination of geometry parameter values  $\xi$  and the error parameter (hyper parameter)  $b$  from measured efficiencies  $y$ .

To obtain a fast evaluation of the surrogate, the function  $f^*$  is expanded into an orthonormal polynomial basis  $\{\Phi_\alpha\}_{\alpha \in \Lambda} \subset L^2(\Omega; \varrho)$ <sup>25-27</sup>

$$f^*(\xi) \approx f(\xi) = \sum_{\alpha \in \Lambda} f_\alpha \Phi_\alpha(\xi) \quad \text{with} \quad f_\alpha = \int_{\Omega} f(\xi) \Phi_\alpha(\xi) d\varrho(\xi). \quad (3)$$

The finite set  $\Lambda \subset \mathbb{N}_0^M$  of cardinality  $P \in \mathbb{N}$  is a set of multiindices and  $\varrho$  denotes the multivariate parameter density for the parameters  $\xi$ . With this surrogate the evaluation of the model in different parameter realizations is equivalent to the evaluation of polynomials.

We want to emphasize, that this approach allows for a global sensitivity analysis of the parameters at almost no additional cost.<sup>?, 17, 28–33</sup>

### 3. OPTIMAL LINEAR REGRESSION

A simple and non-intrusive approach to compute the expansion coefficients in (3) is linear regression. With the reasonable assumption that, for an arbitrary enumeration of  $\Lambda$ , the residuum  $\mathcal{R}(\xi) = f^*(\xi) - \sum_{\ell=1}^P f_\ell \Phi_\ell(\xi)$  is a zero mean random variable, we want to find coefficients that minimize the variance of the residuum  $\mathcal{R}$ . In other words, we obtain the least-squares minimization problem:

$$\text{Find coefficients } f_\ell, \ell = 1, \dots, P \text{ such that } \int_{\Omega} \mathcal{R}(\xi)^2 d\varrho(\xi) = \min. \quad (4)$$

To avoid the high dimensional numerical integration in (4), we approximate the integral in a Monte Carlo sense by

$$\int_{\Omega} \mathcal{R}(\xi)^2 d\varrho(\xi) \approx \frac{1}{N} \sum_{i=1}^N \mathcal{R}(\xi^{(i)})^2, \quad (5)$$

where  $\xi^{(1)}, \dots, \xi^{(N)}$  are  $N$  realizations of possible geometry parameter values (see the domain column in Tab. 1). Since (4) is a quadratic minimization problem, the critical point of the first variation yields the wanted minimum. This critical point can be obtained by solving the linear system

$$F = (\Psi^T \Psi)^{-1} \Psi^T F^*, \quad (6)$$

where the matrices  $\Psi$  and  $F^*$  are given by  $\Psi_{i\ell} = \Phi_\ell(\xi^{(i)})$  and  $F_i^* = f^*(\xi^{(i)})$ . To guarantee that the empirical Gramian  $\Psi^T \Psi$  is not ill-conditioned, the number of realizations  $N$  has to be sufficiently large. The choice of sampling points is in principle arbitrary, but Cohen and Migliorati<sup>34</sup> showed, that sampling from a specific weighted least-squares distribution leads to an optimal (minimal) number of samples for a guaranteed well-conditioned Gramian matrix. Hence, we set

$$d\mu = w^{-1} d\varrho \quad \text{for} \quad w^{-1}(\xi) = \frac{1}{P} \sum_{\ell=1}^P |\Phi_\ell(\xi)|^2 \quad (7)$$

and draw samples  $\xi^{(i)} \sim \mu$ . Note that  $\mu$  is still a probability measure since the polynomials  $\{\Phi_\ell\}$  are orthogonal and normalized. With this, the number of samples required to guarantee a low condition of the Gramian reads  $N/\log(N) \geq cP$  for some  $c > 0$ . Here, we choose  $c = 4$ , motivated by the empirical results in.<sup>34</sup>

Applying this optimal sampling strategy allows us to compute a surrogate for the forward model using a minimal number of function evaluations. This surrogate will be employed to reconstruct geometry parameters and quantify the reconstruction uncertainties using Bayesian inference.

#### 4. BAYESIAN APPROACH

The Bayesian approach provides a statistical method to solve the inverse problem. Following Bayes' theorem, the posterior density is given by

$$\pi(\hat{\xi}; y) = \frac{\mathcal{L}(\hat{\xi}; y)\pi_0(\hat{\xi})}{\int \mathcal{L}(\hat{\xi}; y)\pi_0(\hat{\xi}) d\hat{\xi}}, \quad (8)$$

where the prior density  $\pi_0$  describes prior knowledge and the likelihood function  $\mathcal{L}$  contains the information obtained from the measurement under the assumption of a specific measurement error model. Since the prior density allows for expert knowledge to influence the model, it has to be chosen appropriately not to introduce a bias on the system. We choose a uniform prior to induce as less information as possible on the compact domains of the geometry parameters. The computational and implementation efforts of the Bayesian approach are higher than for the maximum likelihood or least squares methods. However, the posterior yields information about the complete probability density function of the geometry parameters and is thus more reliable for the determination of uncertainties than merely using quantities such as mean and covariance. In addition, the combination of the results from different measurement modalities within the Bayesian framework assures a consistent propagation of uncertainties through all measurement contributions<sup>35,36</sup> (hybrid metrology) in a way that the posterior for one measurement can be used as the prior for the next.

Table 1. Estimations of parameters and uncertainties obtained from the mean value (mean), the double standard deviation ( $2\sigma$ ), relative double standard deviation (11) (rel- $2\sigma$ ), skewness (skew) and kurtosis of the posterior distribution. The domain indicates the support of the prior distribution chosen.

parameter	domain	mean	$2\sigma$	rel- $2\sigma$	skew	kurtosis
$h$ / nm	[43.0, 53.0]	48.35	3.11	0.6224	-0.0518	2.23
cd / nm	[22.0, 28.0]	25.48	0.59	0.1981	0.0188	5.49
swa / °	[84.0, 90.0]	86.87	2.65	0.8847	-0.0172	2.14
$t$ / nm	[4.0, 6.0]	4.96	0.35	0.3511	0.0074	2.93
$r_{\text{top}}$ / nm	[8.0, 13.0]	10.65	2.30	0.9202	-0.0466	2.14
$r_{\text{bot}}$ / nm	[3.0, 7.0]	4.89	1.80	0.8991	-0.0482	2.11
$b$	[0.0, 0.1]	0.01	0.0042	0.1698	1.0199	17.51

The vector  $\hat{\xi}$  consists of geometry parameters  $\xi$  and the noise parameter, i.e.  $\hat{\xi} = (\xi, b)$ . Assuming normal distributed zero-mean measurement errors, we choose the likelihood function<sup>37</sup>

$$\mathcal{L}(\hat{\xi}; y) = \prod_{j=1}^d \frac{1}{\sqrt{2\pi}\sigma_j(b)} \exp\left(-\frac{(f^{(j)}(\xi) - y_j)^2}{2\sigma_j^2(b)}\right), \quad (9)$$

where  $f^{(j)}$  is the  $j$ -th component of (the vector valued function)  $f$ . Note that the form of the measurement error has to be chosen appropriately not to introduce a bias. A more general approach in our case would be not to impose a zero mean but introduce another random hyper parameter. However, the residuum in Fig. 4 suggests that the noise is distributed around zero. In the Bayesian framework, the distributions of parameters are in general determined by Markov-Chain Monte Carlo (MCMC) sampling where for every sampling step, the forward model has to be evaluated. Normally, this means that equation (1) has to be solved which makes MCMC sampling impractical due to the large number of required sampling steps. Since the surrogate only requires evaluations of polynomials, the Bayesian approach becomes practical for scatterometry measurement evaluations.<sup>20</sup>

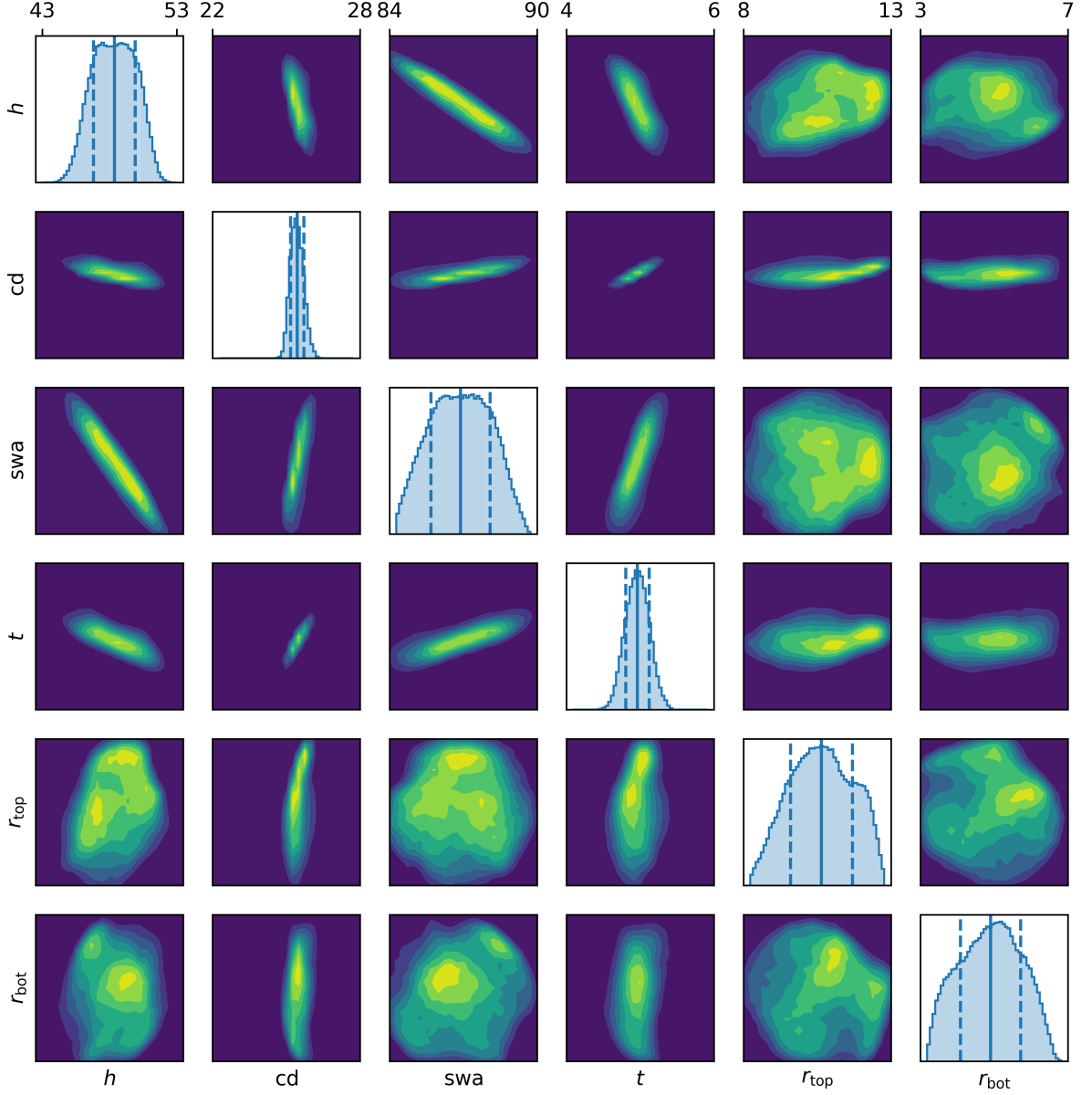


Figure 2. Marginal 1D and 2D densities for the posterior of the stochastic parameters. For the 1D densities, the mean (solid line) and the standard deviation (dashed line) are depicted as well.

For Bayesian inversion, we have to choose a prior distribution for the parameters, calculate the likelihood function and determine the corresponding posterior distribution. The posterior distribution contains the desired parameter values and their associated uncertainties. When two or more measurement results from different measurement sets  $y^{(1)}, \dots, y^{(K)}$  are combined, the posterior distribution of the first measurement can be used as the prior distribution for the evaluation of the second measurement, i.e.

$$\pi(\hat{\xi}; y^{(K)}, y^{(K-1)}, \dots, y^{(1)}) = \frac{\pi_0(\hat{\xi}) \prod_{k=1}^K \mathcal{L}(\hat{\xi}; y^{(k)})}{\int \pi_0(\hat{\xi}) \prod_{k=1}^K \mathcal{L}(\hat{\xi}; y^{(k)}) d\hat{\xi}}. \quad (10)$$

Note that the model function  $f$  in the likelihood function is in general different for different measurement

setups.

## 5. RESULTS

First we want to emphasize the efficiency of our approach. For the scattering problem at hand, it is sufficient to use a chaos expansion with 217 terms to achieve a relative empirical  $L^2$ -error of less than 1%. Therefore, in the sense of section 3, we generate approximately  $10^4$  samples for the FEM forward model to evaluate. In comparison, the computation of the function mean, variance and Sobol indices or the generation of posterior samples, if done empirically, require more than  $10^6$  function evaluations each due to the slow convergence rate of Monte Carlo integration.

We apply Bayesian inversion to the scatterometry measurements to estimate geometry parameters of the line grating. More details of the measurement setup are described in previous works.<sup>5,15</sup> A global sensitivity analysis for the geometry parameters<sup>33</sup> indicates that the reconstruction of all parameters is possible, i.e. the forward model is sensitive to all of them. In particular, the oxide layer thickness and critical dimension should be possible to determine precisely due to their high sensitivity.

For Bayesian inversion it is necessary to chose prior distributions. In our investigations we have chosen uniform priors on the domains given in Table 1. To obtain the posterior distribution, we sampled with an MCMC random walk Metropolis-Hastings algorithm using the surrogate. We have chosen a sampling size of  $10^6$  samples and a burn in phase of  $10^4$  samples. For diagnostics, we applied the Gelman-Rubin criterion,<sup>38</sup> to assure that the chains have fully explored the posterior.

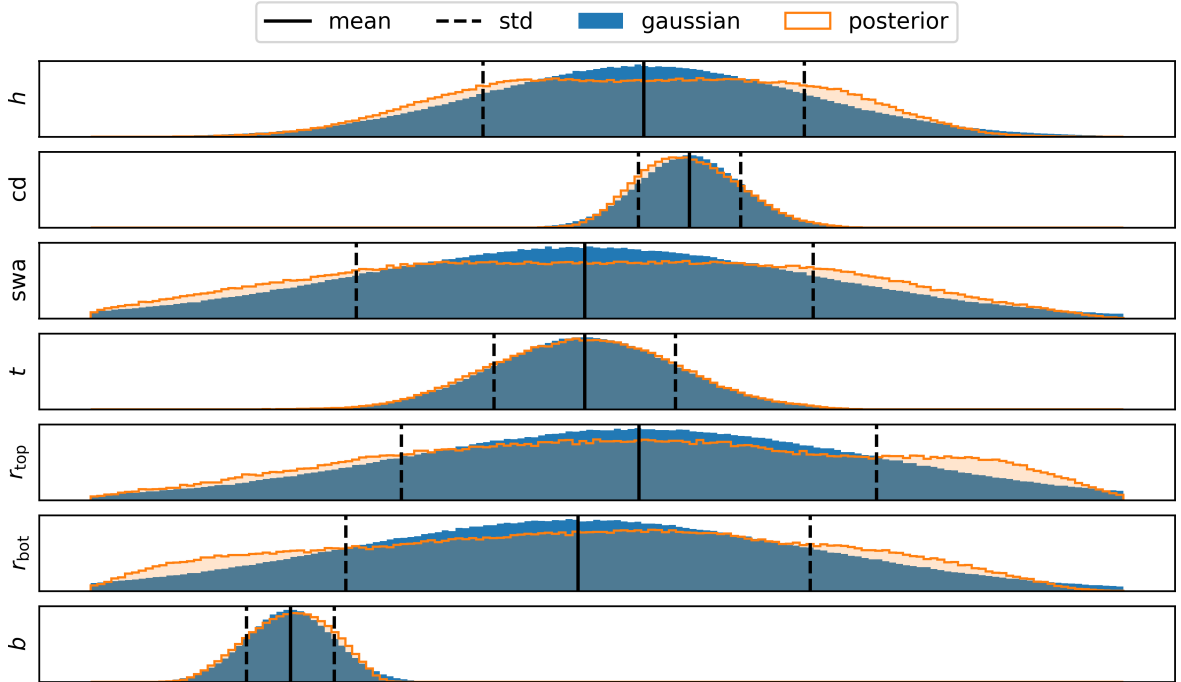


Figure 3. Deviation of posterior marginals from Gaussian distribution with the same mean and variance. The distributions are depicted in their respective reconstruction domains (see Table 1).

In Fig. 2 the posterior (marginal) densities for all 6 stochastic parameters are shown. All posterior densities are characterized by sharp peaks with mean and standard deviation similar to the previous publication.<sup>15</sup> The mean and double standard deviation for each parameter including the hyperparameter (error parameter)  $b$  are shown in Table 1. Since the domain sizes of the parameters vary due to their geometrical meaning, we introduce the relative double standard deviation ( $\text{rel-}2\sigma$ ). The  $\text{rel-}2\sigma$  of a stochastic variable  $\eta$  is the double standard deviation divided by half the width of the parameter domain:

$$\text{rel-}2\sigma = \frac{4\sigma}{\beta - \alpha} \quad \text{where } \eta \in [\alpha, \beta]. \quad (11)$$

The rel- $2\sigma$  shows how the posterior distribution is spread within the domain. For example, if the domain for the critical dimension is [22, 28] nm, and the  $2\sigma$  is 0.6 nm then the rel- $2\sigma$  is 0.198, i.e. the posterior distribution is concentrated in about 20% of the originally chosen domain. This way we can deduce how wide the parameter distributions are spread across the reconstruction domains. The rel- $2\sigma$  in Table 1 shows that the smallest reconstruction uncertainties are obtained for the critical dimension with rel- $2\sigma$  about 20%, followed by the oxide layer thickness with 35% rel- $2\sigma$ . The height has a rel- $2\sigma$  of about 62%. The posterior densities of the sidewall angle and the corner rounding are slightly wider distributed at about 90% rel- $2\sigma$ . This goes in line with the global sensitivity analysis.<sup>33</sup> The results for the error parameter  $b$  depicted in Table 1 show that the relative measurement uncertainty is approximately 1%.

One major advantage of the Bayesian inference is information about the complete posterior distribution instead of just parameter values obtained from the global minimizer. Looking at the marginals in Fig. 2, it is easy to verify that the posterior is not Gaussian. The densities of the rounding radii are not symmetric, the marginal distribution of the sidewall angle exhibits a plateau around the mean and the height even suggests multi-modalities. Another validation of these observations can be found in the skewness (third moment) and kurtosis (fourth moment) of the posterior. These differ (except for the oxide layer thickness) quite significantly from the skewness and kurtosis of a Gaussian, see Table 1. The deviation of the marginals from a Gaussian with the same mean and standard deviation is shown in Fig. 3 for all parameters.

In our case the marginal distributions of the posterior are similar enough to a Gaussian distribution that the  $2\sigma$  confidence interval contains roughly 95% of the mass, as displayed in Table 2. However, in general it is more reasonable to directly compute intervals of mass concentration (confidence intervals) rather than relying on the standard deviation to characterize the uncertainties of a distribution, because this can be misleading for non-Gaussian distribution shapes occurring for example in.<sup>20,39</sup>

Table 2. Double standard deviation and 95% mass confidence intervals of all geometry parameters and the error hyperparameter.

parameter	$2\sigma$ interval	95% confidence interval
$h$ / nm	(45.24, 51.47)	(45.46, 51.13)
cd / nm	(24.88, 26.07)	(24.95, 26.09)
swa / °	(84.22, 89.52)	(84.43, 89.27)
$t$ / nm	(4.61, 5.31)	(4.61, 5.30)
$r_{\text{top}}$ / nm	(8.35, 12.96)	(8.51, 12.67)
$r_{\text{bot}}$ / nm	(3.09, 6.69)	(3.26, 6.49)
$b$	(0.0054, 0.0139)	(0.0056, 0.0133)

Finally, Fig. 4 displays a comparison between the measurement data and the evaluation of our surrogate model using reconstructed geometry parameters. The pointwise relative deviation of the approximation from the measurement data is 2% and lower. This is in accordance with the reconstructed value of  $b$ , which describes the mismatch between the surrogate of the forward model  $f$  and the measurements. In a previous work<sup>15</sup> a Maximum Posterior Approach (MPA) incorporating the same measurement data was used to determine the geometry parameters. The MPA searches for the global maximum of the posterior. Uncertainties were determined locally with an approximation of the covariance matrix around the maximum posterior point. The difference here is that we calculated the whole posterior distribution. This has the advantage that even for multiple peaked and non-Gaussian posterior distributions this scheme gives reliable uncertainty estimations. The results obtained in<sup>15</sup> are consistent to our findings since the posterior is relatively close to the assumed Gaussian shape. There are



only slight differences. For example, the marginal distribution for the height  $h$  is broad (non-Gaussian) yielding larger uncertainties. Similarly, the mean values for  $r_{\text{top}}$  and  $r_{\text{bot}}$  are slightly shifted due to the asymmetry of the marginal posterior (non-Gaussian). The deviation between the forward model values and the measurement data of 2% is comparable with that found in.<sup>15</sup>

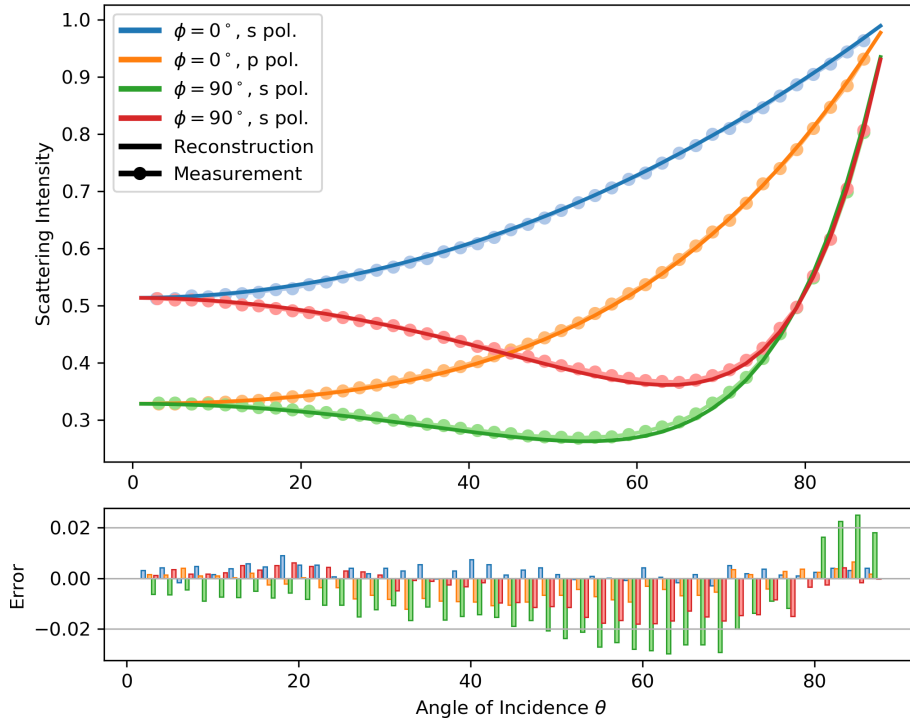


Figure 4. Scattered intensities for the two polarizations and different azimuthal angles. Compared are the measurements of the scatterometry experiment and the simulation of the PC surrogate for the mean values of the parameter reconstruction. The bottom graph shows the pointwise deviation.

## 6. CONCLUSION

In this paper we applied a polynomial chaos expansion as a surrogate for the forward model in scatterometry. Since the surrogate only requires the evaluation of polynomials instead of solving Maxwell’s equation, it was feasible to use a full Bayesian approach to determine the posterior distribution for all geometry parameters. To generate samples from the posterior distribution, we employed a MCMC Metropolis random walk sampling method and checked the overall independence of the samples obtained by the Gelman-Rubin criterion. The reconstruction results obtained by the surrogate model compared to those obtained by a Maximum Posterior estimate with a Gauss-Newton like method<sup>15</sup> are consistent and are in line with the predictions from a global sensitivity analysis. We conclude that a Bayesian approach based on the polynomial chaos surrogate gives accurate and reliable estimations for silicon line grating parameters and uncertainties.

## REFERENCES

- [1] Hsu, S. and Terry, F., “Spectroscopic ellipsometry and reflectometry from gratings (scatterometry) for critical dimension measurement and in situ, real-time process monitoring,” *Thin Solid Films* **455**, 828–836 (2004).
- [2] Mack, C., [*Fundamental principles of optical lithography: the science of microfabrication*], John Wiley & Sons (nov 2008).

- [3] Scholze, F., Soltwisch, V., Dai, G., Henn, M.-A., and Gross, H., “Comparison of CD measurements of an EUV photomask by EUV scatterometry and CD-AFM,” in [*Photomask Technology 2013*], **8880**, 88800O, International Society for Optics and Photonics (2013).
- [4] Henn, M.-A., Gross, H., Heidenreich, S., Scholze, F., Elster, C., and Bär, M., “Improved reconstruction of critical dimensions in extreme ultraviolet scatterometry by modeling systematic errors,” *Measurement Science and Technology* **25**(4), 044003 (2014).
- [5] Wurm, M., Bonifer, S., Bodermann, B., and Richter, J., “Deep ultraviolet scatterometer for dimensional characterization of nanostructures: system improvements and test measurements,” *Measurement Science and Technology* **22**(9), 094024 (2011).
- [6] Agocs, E., Bodermann, B., Burger, S., Dai, G., Endres, J., Hansen, P.-E., Nielson, L., Madsen, M. H., Heidenreich, S., Krumrey, M., et al., “Scatterometry reference standards to improve tool matching and traceability in lithographical nanomanufacturing,” in [*Nanoengineering: Fabrication, Properties, Optics, and Devices XII*], **9556**, 955610, International Society for Optics and Photonics (2015).
- [7] Wurm, M., Endres, J., Probst, J., Schoengen, M., Diener, A., and Bodermann, B., “Metrology of nanoscale grating structures by UV scatterometry,” *Optics express* **25**(3), 2460–2468 (2017).
- [8] Raymond, C. J., Murnane, M. R., Sohail, S., Naqvi, H., and McNeil, J. R., “Metrology of subwavelength photoresist gratings using optical scatterometry,” *Journal of Vacuum Science & Technology B: Microelectronics and Nanometer Structures Processing, Measurement, and Phenomena* **13**(4), 1484–1495 (1995).
- [9] Madsen, M. H. and Hansen, P.-E., “Imaging scatterometry for flexible measurements of patterned areas,” *Optics express* **24**(2), 1109–1117 (2016).
- [10] Paz, V. F., “Solving the inverse grating problem by white light interference fourier scatterometry,” *Light: Science & Applications* **1**(11), e36 (2012).
- [11] Germer, T. A., Patrick, H. J., Silver, R. M., and Bunday, B., “Developing an uncertainty analysis for optical scatterometry,” in [*Metrology, Inspection, and Process Control for Microlithography XXIII*], **7272**, 72720T, International Society for Optics and Photonics (2009).
- [12] Orji, N. G., Badaroglu, M., Barnes, B. M., Beitia, C., Bunday, B. D., Celano, U., Kline, R. J., Neisser, M., Obeng, Y., and Vladar, A., “Metrology for the next generation of semiconductor devices,” *Nature electronics* **1**(10), 532 (2018).
- [13] El Gawhary, O., Kumar, N., Pereira, S., Coene, W., and Urbach, H., “Performance analysis of coherent optical scatterometry,” *Applied Physics B* **105**(4), 775–781 (2011).
- [14] Henn, M.-A., Gross, H., Scholze, F., Wurm, M., Elster, C., and Bär, M., “A maximum likelihood approach to the inverse problem of scatterometry,” *Opt. Express* **20**(12), 12771–12786 (2012).
- [15] Hammerschmidt, M., Weiser, M., Santiago, X. G., Zschiedrich, L., Bodermann, B., and Burger, S., “Quantifying parameter uncertainties in optical scatterometry using Bayesian inversion,” in [*Modeling Aspects in Optical Metrology VI*], Bodermann, B., Frenner, K., and Silver, R. M., eds., **10330**, 8 – 17, International Society for Optics and Photonics, SPIE (2017).
- [16] Heidenreich, S., Gross, H., Wurm, M., Bodermann, B., and Bär, M., “The statistical inverse problem of scatterometry: Bayesian inference and the effect of different priors,” in [*Modeling Aspects in Optical Metrology V*], **9526**, 95260U, International Society for Optics and Photonics (2015).
- [17] Sudret, B., “Global sensitivity analysis using polynomial chaos expansions,” *Reliability Engineering and System Safety* **93**(7), 964–979 (2008).
- [18] Xiu, D., “Fast numerical methods for stochastic computations: A review,” *Commun. Comput. Phys* **5**, 242–272 (2009).
- [19] Heidenreich, S., Gross, H., Henn, M., Elster, C., and Bär, M., “A surrogate model enables a bayesian approach to the inverse problem of scatterometry,” in [*Journal of Physics: Conference Series*], **490**(1), 012007, IOP Publishing (2014).
- [20] Heidenreich, S., Gross, H., and Bär, M., “Bayesian approach to determine critical dimensions from scatterometric measurements,” *Metrologia* **55**(6), S201 (2018).
- [21] Monk, P., [*Finite element methods for Maxwell’s equations*], Numerical Mathematics and Scientific Computation, Oxford University Press, New York (2003).

- [22] Pomplun, J., Burger, S., Zschiedrich, L., and Schmidt, F., “Adaptive Finite Element Method for Simulation of Optical Nano Structures,” *Physica Status Solidi (B)* **244**, 3419–3434 (oct 2007).
- [23] Berenger, J.-P., “A perfectly matched layer for the absorption of electromagnetic waves,” *Journal of Computational Physics* **114**(2), 185–200 (1994).
- [24] Zschiedrich, L., *Transparent boundary conditions for Maxwells equations: numerical concepts beyond the PML method*, phd thesis, Freie Universität Berlin (2009).
- [25] Wiener, N., “The Homogeneous Chaos,” *Amer. J. Math.* **60**(4), 897–936 (1938).
- [26] Cameron, R. H. and Martin, W. T., “The orthogonal development of non-linear functionals in series of Fourier-Hermite functionals,” *Ann. of Math. (2)* **48**, 385–392 (1947).
- [27] Ghanem, R. and Spanos, P.-T., “Polynomial chaos in stochastic finite elements,” *Journal of Applied Mechanics-Transactions of The Asme - J APPL MECH* **57**, 197–202 (03 1990).
- [28] Sobol, I. M., “Sensitivity estimates for nonlinear mathematical models,” *Math. Modeling Comput. Experiment* **1**(4), 407–414 (1995) (1993).
- [29] Sobol, I. M., “Global sensitivity indices for nonlinear mathematical models and their Monte Carlo estimates,” *Math. Comput. Simulation* **55**(1-3), 271–280 (2001).
- [30] Homma, T. and Saltelli, A., “Importance measures in global sensitivity analysis of nonlinear models,” *Reliability Engineering and System Safety* **52**(1), 1–17 (1996).
- [31] Saltelli, A. and Annoni, P., “How to avoid a perfunctory sensitivity analysis,” *Environmental Modelling and Software* **25**(12), 1508 – 1517 (2010).
- [32] Saltelli, A., Annoni, P., Azzini, I., Campolongo, F., Ratto, M., and Tarantola, S., “Variance based sensitivity analysis of model output. design and estimator for the total sensitivity index,” *Computer Physics Communications* **181**(2), 259 – 270 (2010).
- [33] Farchmin, N., Hammerschmidt, M., Schneider, P.-I., Wurm, M., Bodermann, B., Bär, M., and Heidenreich, S., “Efficient global sensitivity analysis for silicon line gratings using polynomial chaos,” in [*Modeling Aspects in Optical Metrology VII*], Bodermann, B., Frenner, K., and Silver, R. M., eds., *Proc. SPIE* **11057**, 115 – 121, International Society for Optics and Photonics, SPIE (2019).
- [34] Cohen, A. and Migliorati, G., “Optimal weighted least-squares methods,” *SMAI Journal of Computational Mathematics* **3**, 181–203 (2017).
- [35] Silver, R. M., Zhang, N. F., Barnes, B. M., Qin, J., Zhou, H., and Dixson, R., “A bayesian statistical model for hybrid metrology to improve measurement accuracy,” in [*Modeling Aspects in Optical Metrology III*], **8083**, 808307, International Society for Optics and Photonics (2011).
- [36] Silver, R. M., Barnes, B. M., Zhang, N. F., Zhou, H., Vladar, A., Villarrubia, J., Kline, J., Sunday, D., and Vaid, A., “Optimizing hybrid metrology through a consistent multi-tool parameter set and uncertainty model,” in [*Metrology, Inspection, and Process Control for Microlithography XXVIII*], **9050**, 905004, International Society for Optics and Photonics (2014).
- [37] Heidenreich, S., Gross, H., and Bär, M., “Bayesian approach to the statistical inverse problem of scatterometry: Comparison of three surrogate models,” *International Journal for Uncertainty Quantification* **5**(6) (2015).
- [38] Gelman, A. and Rubin, D. B., “Inference from iterative simulation using multiple sequences,” *Statistical Science* **7**(4), 457–472 (1992).
- [39] Fernández Herrero, A., Pflüger, M., Probst, J., Scholze, F., and Soltwisch, V., “Applicability of the debye-waller damping factor for the determination of the line-edge roughness of lamellar gratings,” *Optics Express* **27**(22), 32490 (2019).